Dynamics of Exploding Plasmas in a Magnetic Field

Guy Dimonte and L. G. Wiley
Lawrence Livermore National Laboratory, Livermore, California 94550
(Received 24 May 1991)

The expansion of laser-ablation plasmas in a magnetic field is studied with a new Faraday-rotation magnetic imaging probe and Fourier-analyzed optical plasma images over a wide range of ion magnetization. Plasma instabilities are observed during the plasma expansion which evolve from short to long wavelengths and significantly affect the magnetic structure.

PACS numbers: 52.35.Qz, 52.35.Py, 52.50.Lp, 52.55.Lf

The collisionless expansion of energetic plasmas in a magnetic field is a rich and complicated phenomenon occurring in laboratory and astrophysical environments. Initially, a diamagnetic cavity forms and expands until the plasma and magnetic pressures equalize. The magnetic containment radius is of order $R_b=(3E_k\mu_0/2\pi B_0^2)^{1/3}$ in mks units, where μ_0 is the free-space permeability, B_0 is the magnetic field, and E_k is the plasma kinetic energy. As the plasma decelerates, Rayleigh-Taylor or lower-hybrid-drift-(LHD-) type instabilities grow to large amplitude, producing flutes which extend well beyond the main plasma cloud. The electrons are magnetized and carry most of the plasma current, whereas the ions supply the kinetic energy and are not necessarily magnetized. Thus, an important dynamical parameter is the directed ion Larmor radius ρ_i relative to R_b.

Complex plasma cavities have been investigated in the laboratory [1–4], the ionosphere [5], and near the Earth's bow shock [6]. The maximum radius of the plasma cloud R_p was found to increase with E_k and decrease with B_0, consistent with magnetic containment [2], but with $R_p\sim 0.5R_b$. Jets extending beyond the main plasma cloud were observed and associated with the magnetic deceleration [1,3,4]. The wave number k perpendicular to **B** of the flutes increased with B_0 in Japanese experiments [3], whereas k was insensitive to B_0 in NRL experiments [4]. According to linear LHD theory [7], the wave number of the most unstable mode $k_{\max}$ and the associated frequency both increase with B_0, but their calculated values are much larger than observed. Similar discrepancies occurred in the AMPTE (active magnetospheric particle tracer explorer) chemical release experiments [5]. The shortcomings of linear theory have motivated particle simulations [8] and nonlinear theories of the plasma evolution [9].

To clarify the discrepancies in the containment radius and instability wavelengths, we have experimentally investigated the expansion of laser-ablation plasmas in a magnetic field. We developed a magneto-optic imaging probe (MIP) using Faraday rotation to measure the magnetic profile continuously in radius and time. Plasma instabilities are investigated by Fourier analyzing digitized optical images. The wave-number spectrum and the magnetic profile are found to evolve significantly during the plasma expansion. The role of ion magnetization is studied by varying E_k, B_0, the ion species, and expansion velocity.

The experiment is shown schematically in Fig. 1. We use the Janus laser at LLNL with energy $E_l<200$ J at 1.06 μm and a 25-ns pulse length. Counterstreaming beams are focused using $f/10$ optics onto spherical targets of CH_2, Li^6H, and Al to produce quasispherical plasmas of different charge-to-mass ratios Z/A. The ion species are determined with a Thomson parabola spectrometer [10]. The ion velocity distribution, mass, and kinetic energy are measured with an angular array of Faraday cups used as time-of-flight analyzers. The plasma parameters for shots with $B_0\neq 0$ are obtained with Faraday cups on similar shots with $B_0=0$. A gated (1.5 ns) imager takes four optical plasma images per shot with a 1.4-mm resolution. A diamagnetic loop and magnetic probes measure the global and local diamagnetism, respectively. The MIP measures a continuous magnetic profile using the Faraday-rotator glass FR-5 [11] (3 mm×3 mm×6 cm) with the long axis oriented radially as shown in Fig. 1. A line-focused (2 mm×6 cm) plane-polarized laser beam (14 mW at 488 nm) traverses the FR-5 parallel to B_0, is analyzed with a polarizer, and is imaged onto a streak camera. The beam polarization rotates in proportion to the magnetic field $B_z(r,t)$ locally in radius, but integrated over the $\delta z\sim 3$ mm path within the glass. Thus the spatial resolution is 3 mm. The magnetic field is generated with two coils of mean radius 11 cm. The background pressure is typically below 10^{-5} Torr.

False-color images of the expanding plasma are shown

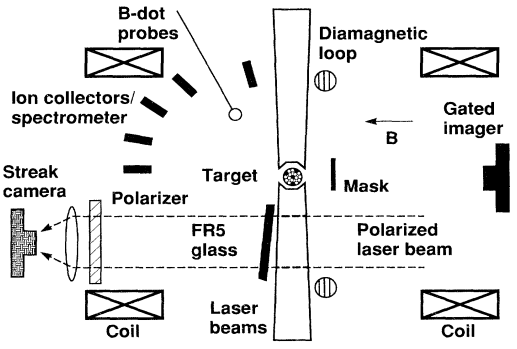

FIG. 1. Schematic of experiment.

© 1991 The American Physical Society

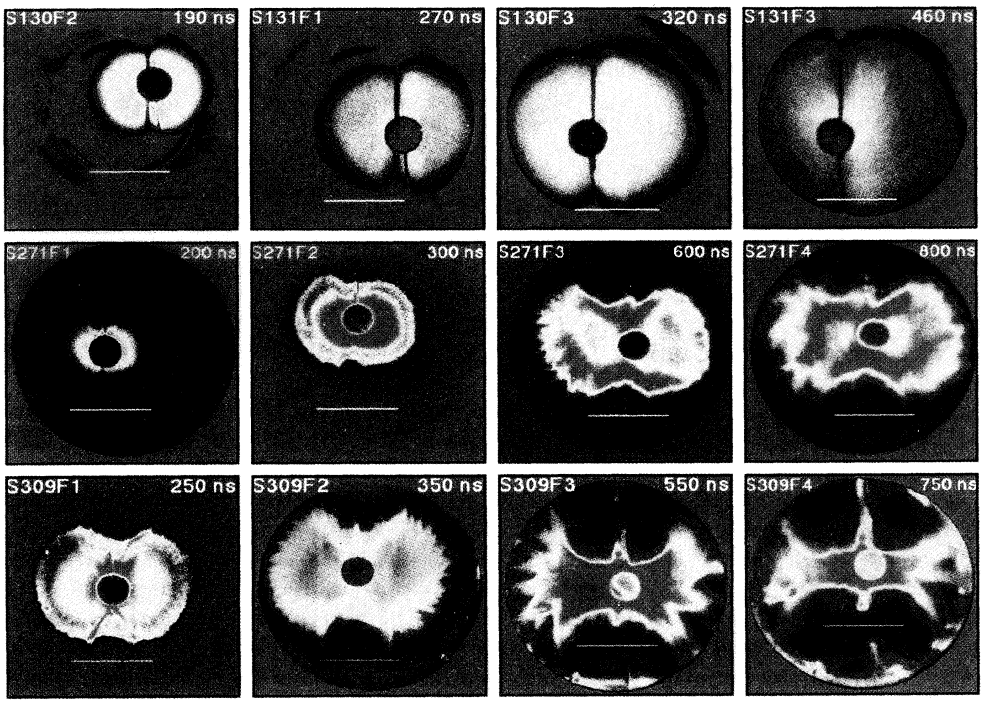

FIG. 2. False-color images of the plasma for three values of magnetic field. **B** points into the paper. Each sequence has four frames during the expansion as indicated. The white lines represent 5 cm.

in Fig. 2. The laser beams enter from the left and right along a horizontal axis and strike a CH_2 sphere of diameter $d=1$ mm for $B_0=0$ and 3 mm for 1 and 3.5 kG. A mask (2 cm diam) protects the imager from the intense glow near the target. The dark vertical lines are the target and mask supports. With $B_0=0$ (shots 130 and 131), the plasma expansion is almost spherical with little structure. The expansion velocities inferred from Faraday cups and Fig. 2(a) agree in magnitude and angular variation, with the average being $v_0\sim 1.8\times 10^7$ cm/s. The velocity spread is typically $0.4v_0$ FWHM. The angular variation of plasma quantities can be approximated by $X(\theta)\sim X_0(1+\varepsilon\cos 2\theta)$ with observed values of $\varepsilon\sim 0.2$, 0.12, and 0.45 for the plasma charge, velocity, and kinetic energy, respectively. The angle θ is with respect to the horizontal laser axis. The total ablated mass is $M_p\sim 0.9$ μg assuming C^{2+} (we observe up to C^{4+}) and the kinetic energy is $E_k\sim 14$ J compared to $E_l\sim 23$ J. The efficiency E_k/E_l varies slightly with laser intensity, target material, and geometry.

With $B_0=3.5$ kG in Fig. 2(c) (shot 309 with $E_l=160$ J, $v_0\sim 1.8\times 10^7$ cm/s, $M_p\sim 6$ μg with C^{2+}, and $E_k\sim 95$ J), the plasma is nearly isotropic initially and becomes highly structured as it decelerates. At the waist ($\theta=90°$), the plasma stagnates first because the energy density is a minimum in azimuth and it is recompressed magnetically by a factor of 2. Along the laser axis, the plasma decelerates but does not recompress, thereby magnifying the initial plasma asymmetries. The time for plasma stagnation correlates well with the time of peak diamagnetic-loop signal, $\tau_{\rm dml}=380$ ns. As the plasma decelerates, flutes develop with short wavelengths initially and long wavelengths later in time. For example, there are approximately 35 flutes in azimuth at $t=350$ ns near stagnation which coalesce to 7 flutes by $t=750$ ns.

Similar behavior is observed in Fig. 2(b) with $B_0=1$ kG (shot 271 with $E_l=13.7$ J, $v_0\sim 9\times 10^6$ cm/s, M_p

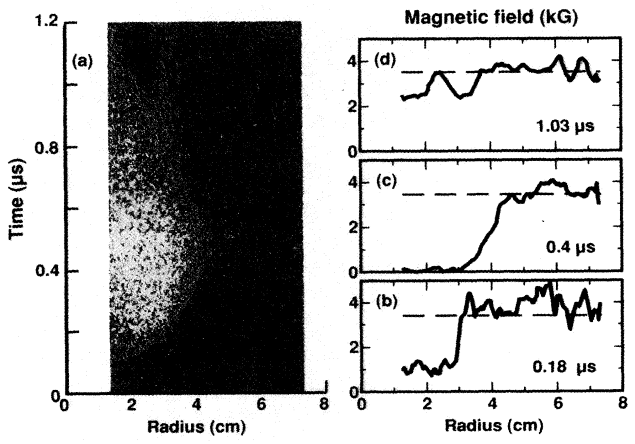

FIG. 3. (a) Streak-camera image from the MIP in false color. The uniform initial field is blue, and the fully diamagnetic cavity is gold. (b)–(d) Radial lineouts for the magnetic profile at different times.

~ 1.4 μg for C^{2+}, and $E_k \sim 6$ J), but the recompression is smaller than with 3.5 kG. The number of flutes also evolves, with ~ 22 flutes at peak diamagnetism $\tau_{dml} = 600$ ns and ~ 14 at $t = 800$ ns.

The evolution of the magnetic-field profile is measured with the MIP as shown in false color in Fig. 3(a). This shot 414 [$B_0 = 3.5$ kG, CH_2 sphere, $d = 3$ mm, $E_l = 117$ J, $v_0 \sim 1.7 \times 10^7$ cm/s, $M_p \sim 5$ μg (C^{2+}), and $E_k \sim 70$ J] is similar to shot 309 in Fig. 2(c). The FR-5 is oriented horizontally near the laser axis. Radial lineouts show the magnetic profiles quantitatively at various times in Figs. 3(b)–3(d). At $t = 0.18$ μs, the cavity is expanding and is not fully diamagnetic. The outer boundary is quite sharp and we cannot resolve the magnetic gradient scale length $L_b \leq 3$ mm. L_b is less than $\rho_i \sim 3$ cm and $c/\omega_{pi} \sim 1$ cm [(speed of light)/(ion plasma frequency)], and may be related to electron or hybrid scale lengths. At $t = 0.4$ μs, the diamagnetic-loop signal has peaked ($\tau_{dml} \sim 0.38$ μs), the cavity has reached its maximum extent, and the boundary is broad. The fully diamagnetic region ($B_z = 0$) has a radius $R_i \sim 3$ cm and the outer cavity radius ($B_z = B_0$) is $R_o \sim 5$ cm. Both are smaller than $R_b \sim 7$ cm. Later, the magnetic field diffuses into the plasma but in an irregular fashion as indicated by the oscillations in Fig. 3(d) which correspond to the red streaks in Fig. 3(a) at $r = 1.5$ and 3 cm for $t > 0.8$ μs. The irregular and broad magnetic structure is correlated with the plasma instability which may be causing the anomalously fast magnetic diffusion of ~ 1 μs compared to the classical magnetic diffusion time ~ 100 μs for 5–10-eV electron temperatures and 2–4-cm magnetic scale lengths.

We now compare the cavity and plasma radii with the magnetic containment radius under varying conditions (B_0, E_l, target size, and ion Li, C, and Al). The maximum magnetic cavity radii R_i and R_o are proportional to R_b as seen in Fig. 4(a) with $R_o \sim 0.75 R_b$ and $R_i \sim 0.5 R_b$. The plasma radii measured photographically at peak diamagnetism are also smaller than R_b as shown in Fig. 4(b). Along the laser axis the plasma radius $R_p \sim 0.75 R_b$, whereas at the waist ($\theta = 90°$) the radius is $R_w \sim 0.5 R_b$. The aspect ratio $R_p/R_w \sim 1.5$ is consistent with the measured azimuthal asymmetry in the plasma kinetic energy since $R_b \sim E_k^{1/3}$. The similarity of R_p and R_o indicate that the plasma is contained within the magnetic cavity up to the time of peak diamagnetism. In Fig. 4(c), we plot R_p and R_o vs ρ_i ($Z = 2$), all scaled to R_b, to assess the importance of ion magnetization. The scaled radius is $R_p/R_b \sim 0.8$ for small ρ_i/R_b and decreases slightly with ion magnetization in qualitative agreement with particle simulations [8] and previous experiments [2] in which the LHD instability was postulated to cause anomalous magnetic diffusion.

The instability structure is evaluated by Fourier analyzing plasma images which are digitized and linearized using calibration wedges. We take a circular lineout at the plasma boundary to obtain the intensity along the circumference $I(x)$, where $x = r\theta$, and Fourier transform it to obtain the spectral intensity $I(k)$. To compare spectra at different times, we normalize each transform by the

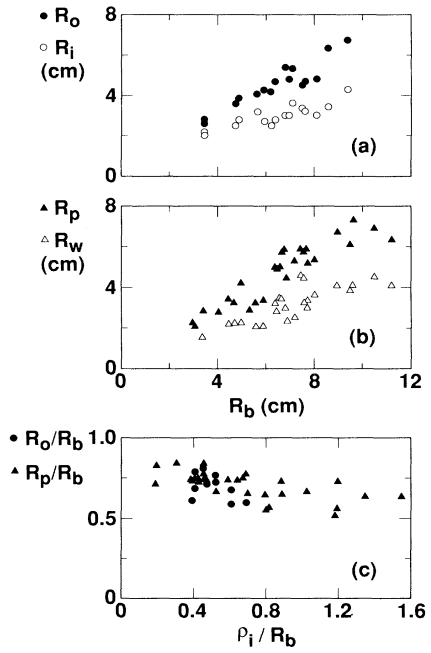

FIG. 4. (a) Inner R_i and outer R_o cavity radii vs R_b. (b) Plasma radii R_p at $\theta = 0$ and R_w at $\theta = 90°$ from gated images at peak diamagnetism. (c) R_o and R_p vs directed ion Larmor radius, all scaled to R_b.

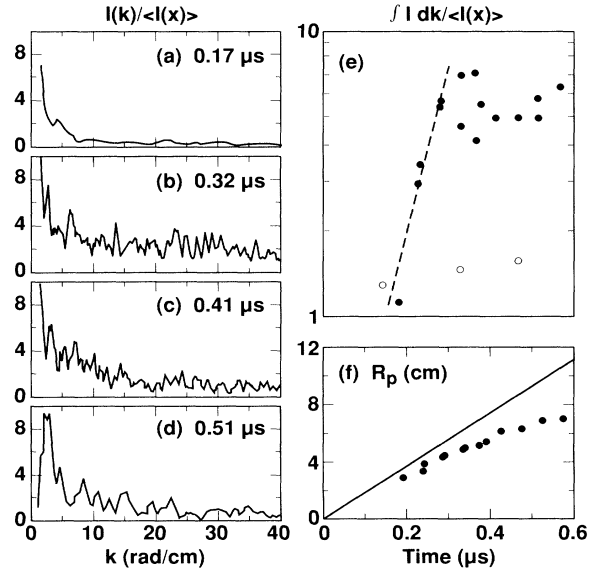

FIG. 5. (a)–(d) Normalized spectra from circular lineouts of digitized plasma images at different times. (e) Integrated spectral amplitude vs time. Open circles are with $B_0 = 0$. (f) Plasma radius from gated images vs time.

average intensity of the lineout $\langle I(x)\rangle$ because the image intensities vary with plasma conditions. The analysis is shown in Fig. 5 for shots 111–116 which are similar to shots 130 and 131 [Fig. 2(a)] but with $B_0=1$ kG. The normalized spectra $I(k)/\langle I(x)\rangle$ are shown at different times in Figs. 5(a)–5(d). For reference, the plasma radius taken from gated images is shown in Fig. 5(f) where the line indicates the measured free streaming trajectory. Early in time $t=0.17$ μs, the spectral intensity is small except for the small initial plasma asymmetry as indicated at small k. At $t=0.32$ μs, $I(k)$ has increased for all wave numbers out to the resolution limit $k\sim 44$ rad/cm. From 0.32 to 0.51 μs, the spectrum evolves, with low-k modes being enhanced at the expense of high-k modes. The evolution toward long wavelengths was seen directly in Fig. 2 with the number of flutes decreasing in time.

To quantify the temporal variation of the instability, we integrate the normalized spectra from $k\sim 2\pi/R_p$ to 44 rad/cm and plot the result in Fig. 5(e) versus time. The lower limit removes the plasma asymmetry and the upper bound is the resolution limit. With $B_0=0$ (shots 130 and 131), the integral is small, consistent with the lack of structure in Fig. 2(a). With $B_0=1$ kG, the integral begins exponential growth at 175 ns and saturates at 325 ns even though the plasma is still decelerating [Fig. 5(f)]. The broad spectrum in Fig. 5(b) is now seen to occur near saturation and the evolution toward small wave numbers occurs in the saturated nonlinear regime.

To compare these results with linear theory [7,8], we evaluate the lower hybrid frequency $\omega_{lh}\sim 1.7\times 10^8$ rad/s, the density gradient scale length $L_n\sim 1$ cm, and an average deceleration $g\sim v_0^2/R_b\sim 3.6\times 10^{13}$ cm/s^2 for the shots in Fig. 5. The most unstable mode has $k_{max}\sim\omega_{lh}/(gL_n)^{0.5}\sim 30$ rad/cm, where the spectrum is finite but not peaked. The growth rate from Fig. 5(e), $\gamma_{exp}\sim 10^7$/s, is much smaller than the theoretical rate $\gamma_{th}\sim\omega_{lh}$ and the calculated rotation frequencies of the unstable modes are much larger than observed. These discrepancies and the analysis in Fig. 5 suggest that a nonlinear theory is required [8,9] particularly since the plasma and the instability evolve on the same time scale.

In conclusion, we have measured the magnetic profile and plasma structure for nearly spherical exploding plasmas in a magnetic field. The diamagnetic cavity and plasma radii scale with the magnetic containment radius over a wide range of ion magnetization. Plasma instabilities are observed which evolve from short to long wavelengths and affect the evolution of the magnetic field.

We thank Dr. S. Brecht, Dr. R. Kilb, Dr. B. H. Ripin, Dr. G. Simonson, and Dr. D. Winske for informative discussions and R. W. Fortner for his support. We also thank G. Vayer, J. Swain, D. Dueree, and G. London for their expert technical assistance. The work was performed under the auspices of the U.S. Department of Energy by the Lawrence Livermore National Laboratory under Contract No. W-7405-ENG-48.

[1] H. Dickinson *et al.*, Phys. Fluids **5**, 1048 (1962).
[2] Yu. P. Zakharov *et al.*, Fiz. Plazmy **12**, 1170 (1986) [Sov. J. Plasma Phys. **12**, 674 (1986)].
[3] S. Okada, K. Sato, and T. Sekiguchi, J. Appl. Phys. **20**, 157 (1981).
[4] B. H. Ripin *et al.*, Phys. Rev. Lett. **59**, 2299 (1987).
[5] P. A. Bernhardt *et al.*, J. Geophys. Res. **92**, 5777 (1987).
[6] M. F. Thomsen *et al.*, J. Geophys. Res. **91**, 2961 (1986).
[7] J. D. Huba, A. B. Hassam, and D. Winske, Phys. Fluids B **2**, 1676 (1990).
[8] D. Winske, Phys. Fluids B **1**, 1900 (1989).
[9] A. B. Hassam and J. D. Huba, Phys. Fluids B **2**, 2001 (1990).
[10] J. P. Anthes, Phys. Teacher **20**, 161 (1982).
[11] A. B. Villaverde and E. C. Vasconcellos, Appl. Opt. **21**, 1347 (1982).

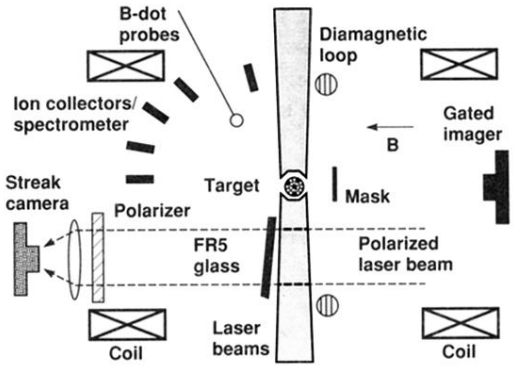

FIG. 1. Schematic of experiment.

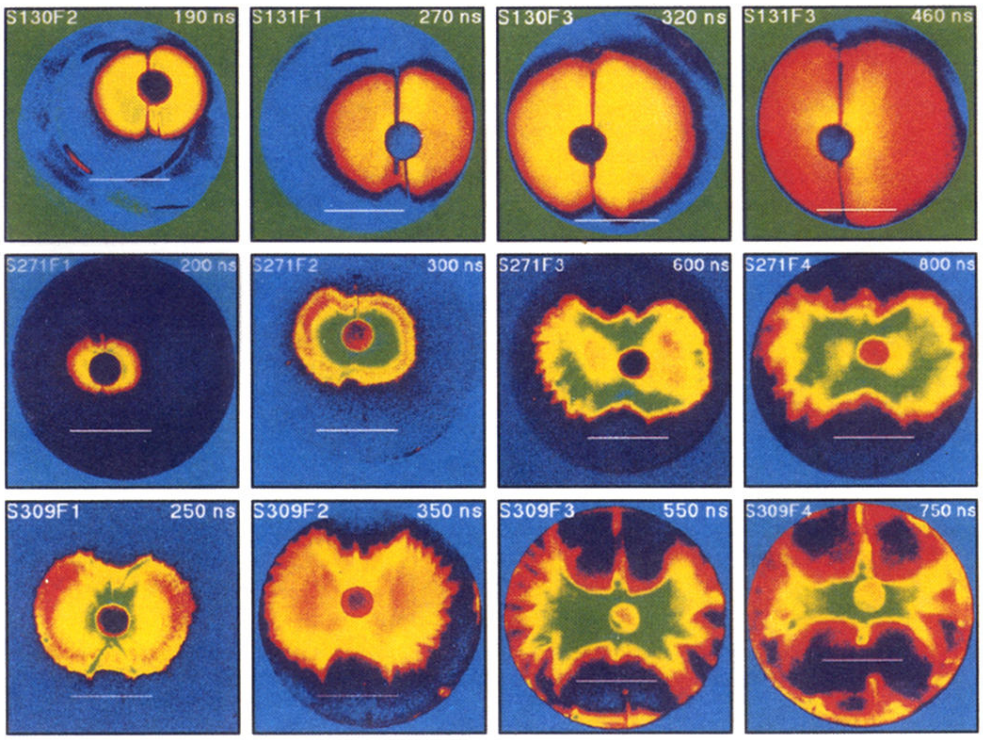

FIG. 2. False-color images of the plasma for three values of magnetic field. **B** points into the paper. Each sequence has four frames during the expansion as indicated. The white lines represent 5 cm.

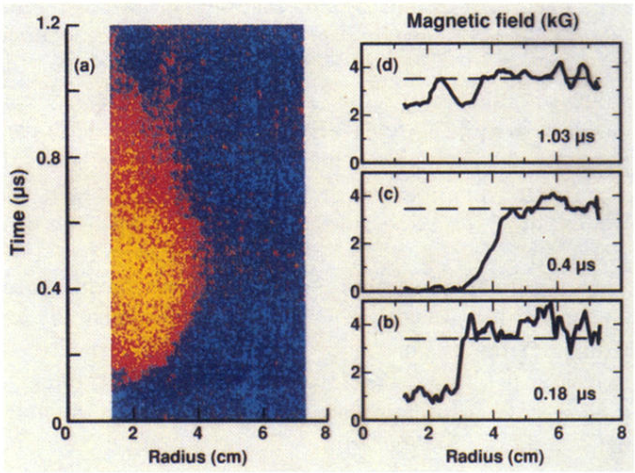

FIG. 3. (a) Streak-camera image from the MIP in false color. The uniform initial field is blue, and the fully diamagnetic cavity is gold. (b)–(d) Radial lineouts for the magnetic profile at different times.